

Article

Equivalence Ratio Measurements in CH₄/Air Gases Based on the Spatial Distribution of the Emission Intensity of Femtosecond Laser-Induced Filament

Ming Li ¹, Jiangpeng Gu ¹, Dayuan Zhang ^{1,2}, Qiang Gao ^{1,*}  and Bo Li ¹

¹ State Key Laboratory of Engines, Tianjin University, Tianjin 300072, China; mingli@tju.edu.cn (M.L.); gujiangpeng@tju.edu.cn (J.G.); dayuan_zhang@tju.edu.cn (D.Z.); boli@tju.edu.cn (B.L.)

² China North Engine Research Institute, Tianjin 300400, China

* Correspondence: qiang.gao@tju.edu.cn; Tel.: +86-136-7202-2787

Abstract: Femtosecond lasers have been used in combustion diagnostics. Based on the characteristics of femtosecond laser filamentation, many diagnostic techniques have been developed. Here, we propose a method, based on femtosecond laser filamentation, for equivalence ratio measurements in CH₄/air gases. By measuring the spatially resolved spectra of the femtosecond laser-induced filament, we found that the variation of the equivalence ratio in the flow field would affect the spatial distribution of the emission intensity of femtosecond laser-induced filament. On this basis, the equivalence ratio was calibrated by using the relative spatial positions of N₂ (337 nm) and C₂ (516.5 nm) signals in the filament. This method overcomes the interference of local air disturbance, having lower measurement uncertainty.

Keywords: femtosecond laser; equivalence ratio; spatially resolved spectrum



Citation: Li, M.; Gu, J.; Zhang, D.; Gao, Q.; Li, B. Equivalence Ratio Measurements in CH₄/Air Gases Based on the Spatial Distribution of the Emission Intensity of Femtosecond Laser-Induced Filament. *Processes* **2021**, *9*, 2022. <https://doi.org/10.3390/pr9112022>

Academic Editor: Zhihua Wang

Received: 13 October 2021

Accepted: 5 November 2021

Published: 12 November 2021

Publisher's Note: MDPI stays neutral with regard to jurisdictional claims in published maps and institutional affiliations.



Copyright: © 2021 by the authors. Licensee MDPI, Basel, Switzerland. This article is an open access article distributed under the terms and conditions of the Creative Commons Attribution (CC BY) license (<https://creativecommons.org/licenses/by/4.0/>).

1. Introduction

Developing advanced combustion diagnostic techniques is crucial in combustion fields. In particular, laser diagnostic technology is playing an increasingly important role in the field of combustion diagnostics because of its advantages such as non-invasive, high sensitivity, high spatial and temporal resolution, real-time, and the ability of simultaneous measurements of multiple parameters [1,2]. The combustion diagnostics based on nanosecond lasers (ns laser) emerged in the 1980s, and many achievements have been made in the measurement of flame structure [3], intermediate products [4], temperature [5] and velocity [6]. In recent years, with the emergence of femtosecond laser [7–9] (fs laser), fs laser diagnostic technology has been applied to combustion fields [10]. Compared with a ns laser, a fs laser has short pulse duration, high peak power, and wide linewidth [1,11]. Owing to these characteristics, the fs laser exhibits many unique phenomena during its propagation, such as spectrum broadening [12], cone radiation [13], population inversion [14], and fs laser filamentation [15]. Among them, fs laser filamentation in the field of combustion diagnostics should attract special attention.

Xu et al. [16] proposed fs filament-induced nonlinear spectroscopy (FINS), which can be used for the measurement of combustion intermediates. On this basis, they [17] compared FINS in flame with ns laser-induced breakdown spectroscopy (ns-LIBS) and flame spontaneous emission spectroscopy and further discussed the applicability of FINS in the measurement of combustion intermediates. Li et al. [18] developed the fs laser-extended electric discharge velocimetry technology by combining fs filamentation and discharge, which has high accuracy in the velocity measurement of flow fields. In addition, Li et al. [19] achieved the temperature measurement of combustion flow fields based on femtosecond laser-induced filament.

The equivalence ratio is an important physical parameter in combustion research. The real-time and accurate equivalence ratio measurements can not only monitor the

combustion process, improve the combustion efficiency [20,21] but also reduce the emission of pollutants [22]. Nanosecond laser-induced breakdown spectroscopy is one of the most commonly used equivalence ratio measurement methods, while the femtosecond laser has advantages over the nanosecond laser due to its low ablation threshold, high temporal and spatial resolution, and low bremsstrahlung interference.

At present, the measurement method of equivalence ratio is mainly based on signal intensity ratio [23], but this method will be disturbed by local air disturbance. In this paper, an equivalence ratio measurement method based on fs filament signal distribution is proposed, which has good precision. This method provides a new idea for measuring the equivalence ratio.

2. Experimental

The schematic of the experimental setup is illustrated in Figure 1. An fs Ti: sapphire laser system (Spitfire Ace, Spectra Physics, Milpitas, CA, USA) was adopted with the output of 800 nm, the pulse duration of ~45 fs, the repetition rate of 1 kHz, and the maximum pulse energy of 7 mJ. The laser pulse energy was adjusted by an attenuator (VA-800-Conex, Thorlabs, Newton, NJ, USA) to 2 mJ/pulse. A McKenna burner was used to generate a premixed laminar CH₄/air gas flow at room temperature. The laser was focused by a spherical lens (f = 500 mm) to form a filament in the gas mixture at 10 mm above the McKenna burner. The equivalence ratio and the gas supply rate of the gas flow were controlled by mass flow controllers. The total gas flow rate, and hence, the gas flow speed were kept constant at $4.24 \times 10^{-4} \text{ m}^3/\text{s}$, and 0.15 m/s, respectively. In order to ensure the stability of the flow field, a low gas flow rate was selected in the experiment. The details of the gas mixture are listed in Table 1.

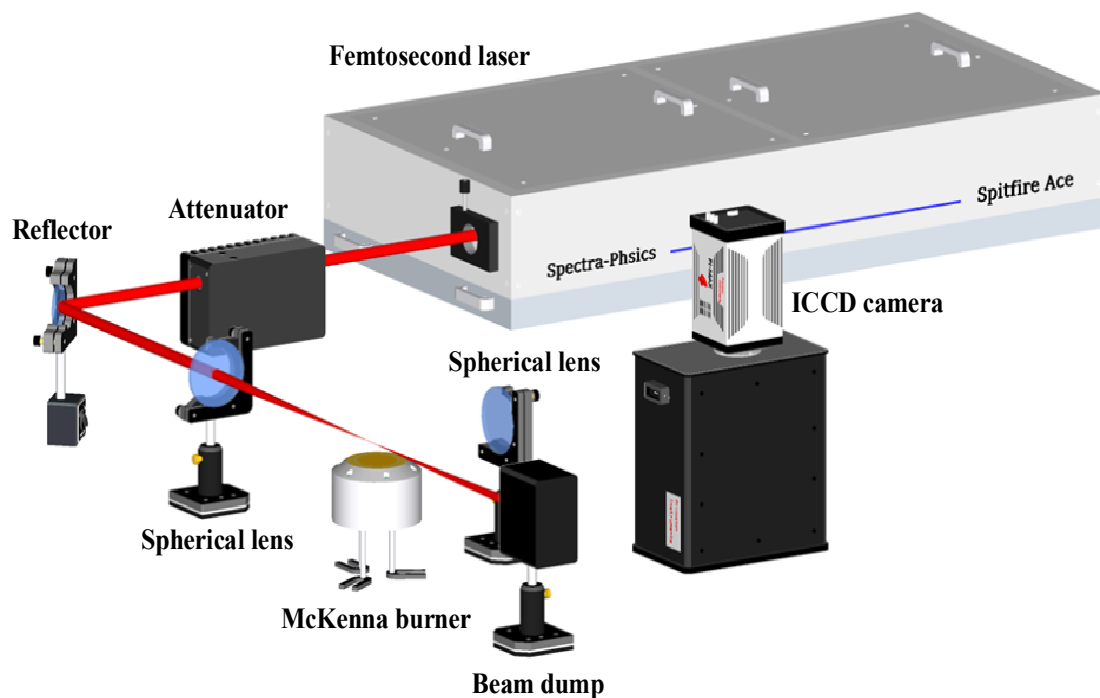


Figure 1. Diagram of experimental setup for equivalence ratio measurement by femtosecond laser-induced filament.

Table 1. CH₄ and air flow rates at different equivalence ratios.

Case	Equivalence Ratio	CH ₄ Flow Rate (10 ⁻⁴ m ³ /s)	Air Flow Rate (10 ⁻⁴ m ³ /s)	Total Flow Rate (10 ⁻⁴ m ³ /s)
1	0.6	0.98	3.26	4.24
2	0.8	1.21	3.03	4.24
3	1	1.41	2.83	4.24
4	1.2	1.59	2.65	4.24
5	1.4	1.75	2.49	4.24
6	1.6	1.88	2.36	4.24

The signal generated by the interaction of the filament and the gas mixture was collected into the input slit (slit width = 200 nm) of a spectrometer (Acton, SP-2300i, Princeton Instruments, Trenton, NJ, USA) by a spherical lens with a focal length of 100 mm. The signal collected by the spectrometer was dispersed by a grating (300 grooves/mm blazed at 300 nm) and then captured by an ICCD camera (PI-MAX4:1024i, Princeton Instruments, Trenton, NJ, USA) coupled with the spectrometer. The input slit of the spectrometer was horizontally arranged (parallel to the filament) to record the spatially resolved spectrum of the filament. The spectral resolution of the spectrometer is 2.53 nm. To ensure the stability of the experiment, we carried out the experiments in a room with constant temperature and pressure. The ambient temperature was 20 °C, the humidity was 50%, and the pressure was 1 atm.

3. Results and Discussion

3.1. Spatially Resolved Spectrum

Firstly, the spatially resolved spectrum of the filament was measured. In the experiment, the gate delay of the camera relative to the laser arrival time was 0 ns, and the camera gate width was 50 ns. The spectrum was an average of 200 laser shots to improve the signal-to-noise ratio. The results are shown in Figure 2.

Figure 2a is the photo of the fs laser filament taken by a single-lens reflex camera (Nikon D90) in a premixed CH₄/air gas mixture with the equivalence ratio of 1. The black arrow shows the laser propagation direction (from left to right). Figure 2b is the spatially resolved spectrum of the filament, and the region of interest is indicated by the red dotted box in Figure 2a. In Figure 2b, the X-axis represents the wavelength, the Y-axis represents the spatial position, and the color bar on the left represents the relative intensity of the signal. The spectral curve in Figure 2c is the integral of the spectrum in Figure 2b. In Figure 2c, the X-axis represents the wavelength, and the Y-axis represents the signal intensity.

In the experiments, the laser with the energy of 2 mJ/pulse was used. When a fs laser is focused with a longer focal length lens, the focused femtosecond laser can form a stable plasma channel in the optical medium. This phenomenon is also known as filamentation, and the plasma channel is called a filament [24]. The appearance of fs filament is due to the dynamic balance between the optical Kerr effect-induced self-focusing and the defocusing effect of the self-generated plasma. The clamping intensity inside the plasma channel induced by fs laser is up to 10¹³~10¹⁴ W/cm², which is intense enough to excite atoms/molecules into higher excited states through photolysis, ionization, dissociation, and collision. Then, the excited atoms/molecules release characteristic fluorescence [1]. In Figure 2c, the characteristic fluorescence can be found, including CH at 314 nm, 388 nm and 431 nm, N₂ at 337 nm and 357 nm, CN at 388 nm, C₂ at 516.5 nm, and H at 656 nm. The energy level transition of the fluorescence signal is shown in Table 2 [25–27].

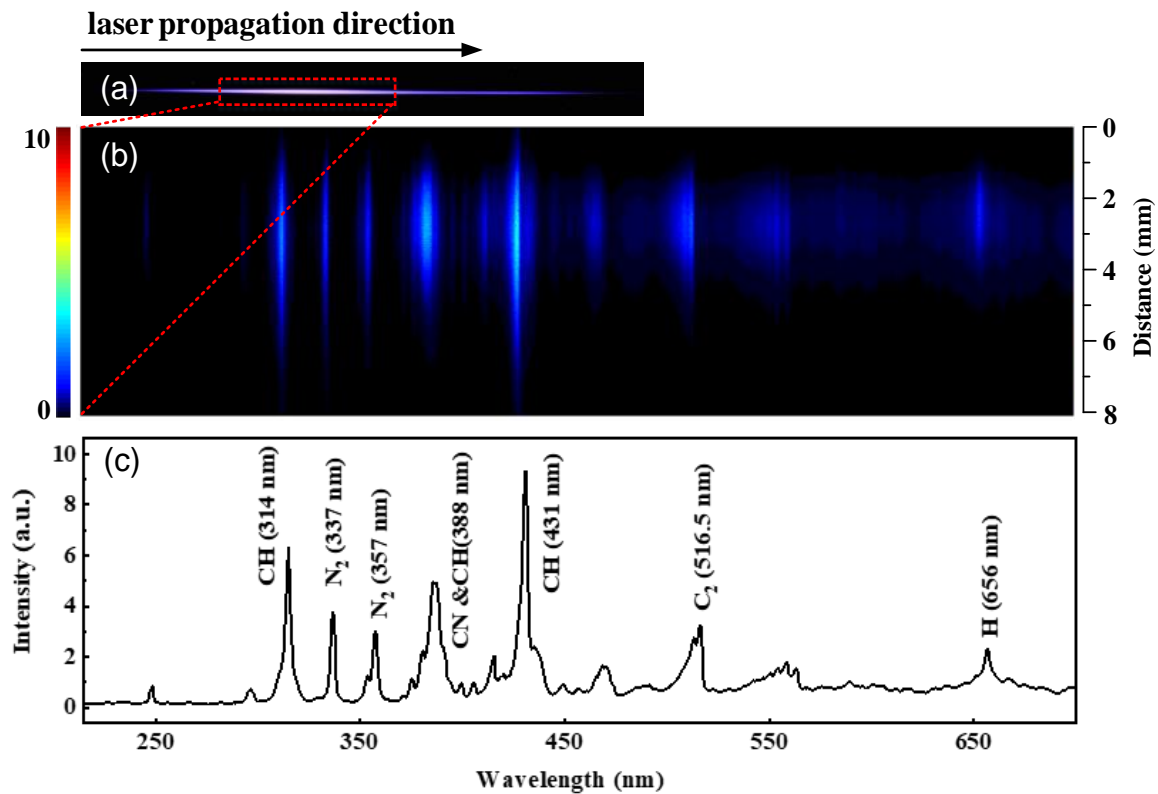


Figure 2. (a), Photo of femtosecond laser filament in a gas mixture. A femtosecond laser was used with a pulse energy of 2 mJ, a wavelength of 800 nm, a pulse duration of ~45 fs and a repetition rate of 1 kHz. The total gas flow rate was $4.24 \times 10^{-4} \text{ m}^3/\text{s}$, the gas flow speed was 0.15 m/s, and the equivalence ratio was 1. (b), the spatially resolved spectral graph of the filament, where the X-axis represents the wavelength, the Y-axis represents the spatial position, and the color bar on the left represents the relative intensity of the signal. (c), the spectral curve obtained from the accumulation of the spectral graph.

Table 2. Energy level transitions of main signals of femtosecond filaments in premixed methane/air mixture.

Component	Wavelength	Transition
CH	~314 nm	$C^2\Sigma^+ - X^2\Pi (0, 0)$
N ₂	~337 nm	$C^3\Pi_u - B^3\Pi_g (0, 0)$
N ₂	~357 nm	$C^3\Pi_u - B^3\Pi_g (0, 1)$
CN	~388 nm	$B^2\Sigma^+ - X^2\Sigma^+ (0, 0)$
CH	~388 nm	$B^2\Sigma^- - X^2\Pi (0, 0)$
CH	~431 nm	$A^2\Delta - X^2\Pi (0, 0)$
C ₂	~516.5 nm	$d^3\Pi_g - a^3\Pi_u (0, 0)$
H	~656 nm	$3p^2P - 2s^2S$

The fluorescence signal of N₂ comes from the transition of the excited state N₂ ($C^3\Pi_u$) to the ground state N₂ ($B^3\Pi_g$). The excited state of N₂ ($C^3\Pi_u$) is mainly generated by the recombination of electrons and ions. The generation process mainly consists of the following three steps [28]. First, N₂ in the ground state is photolyzed by the fs laser into N₂⁺ and e⁻ through Equation (1). Then, N₂⁺ reacts with N₂ to form N₄⁺ through Equation (2). Finally, the excited state N₂ ($C^3\Pi_u$) is produced by N₄⁺ and e⁻ through Equation (3).





C_2 is mainly derived from CH_4 [29]. Through the action of filament, hydrocarbons undergo a series of recombination and dehydrogenation reactions, generating C_2 in the excited state. The excited C_2 transitions to the ground state and emits fluorescence at 516.5 nm. CH radicals and H radicals are two active components, and their generation processes involve multiple chemical reaction paths, which are related to both CH_4 and air in the mixture [29]. The generation process of CN radical is complicated, involving a variety of chemical reactions related to CH_4 and N_2 [30,31].

3.2. Equivalence Ratio Measurements Based on the Emission Intensity Ratio between Two Species in the fs Laser-Induced Filament

In order to explore the influence of the equivalence ratio on the fluorescence signal intensity, systematic experiments were carried out in premixed CH_4/air mixtures with different equivalence ratios. Under the condition that the total gas supply flow rate was $4.24 \times 10^{-4} \text{ m}^3/\text{s}$, six working conditions with the equivalence ratios ranging from 0.6 to 1.6 were selected to obtain the fluorescence spectra. The flow rates of CH_4 and air at different equivalence ratios are shown in Table 1, and the fluorescence spectra at different equivalence ratios are shown in Figure 3.

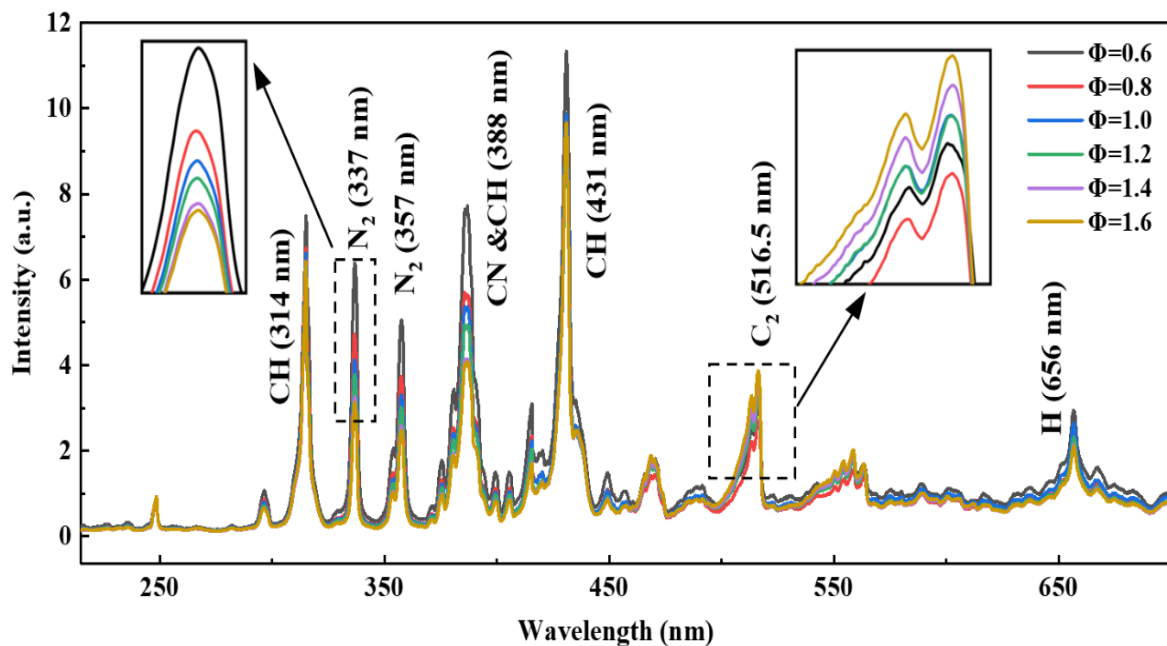


Figure 3. Spectral curves of fs laser-induced filament in CH_4/air mixture at different equivalence ratios. The insets show the locally enlarged view of the N_2 (337 nm) and C_2 (516.5 nm) signals.

In Figure 3, the X-axis represents the wavelength, and the Y-axis represents the intensity of the spectrum. The inset on the left shows the locally enlarged view of the N_2 signal at 337 nm, and the right inset shows the locally enlarged view of the C_2 signal at 516.5 nm. It can be seen that the change of the equivalence ratio only changes the intensity of the spectrum, while the shape of the spectrum does not change. It can be found in these inserts in Figure 3 that with the increase of the equivalence ratio, the signal intensity of N_2 (337 nm) gradually decreases, while the signal intensity of C_2 (516.5 nm) gradually increases. It can be seen from the above that the equivalence ratio is related to the intensity of the fluorescence signal, and the relationship between the equivalence ratio and the fluorescence signal intensity can be used to measure the equivalence ratio [23].

Figure 4 shows the variation trend of N_2 (337 nm) signal intensity and C_2 (516.5 nm) signal intensity as a function of the equivalence ratio, in which signal intensity is repre-

sented by the peak value of the signal intensity. The X-axis represents the equivalence ratio, and the Y-axis represents the intensity. As can be seen from Figure 4, with the increase of the equivalence ratio, the signal intensity of N_2 (337 nm) shows a downward trend, while the signal intensity of C_2 (516.5 nm) shows an upward trend. This is because that as the equivalence ratio increases, the concentration of N_2 (337 nm) decreases, and the concentration of C_2 (516.5 nm) increases. However, the C_2 (516.5 nm) signal intensity shows an oscillatory behaviour with the equivalence ratio. We believe the main reason is local air disturbance. During the measurement process, some air is mixed into the mixture, which will disturb the flow field and affect the spectral intensity.

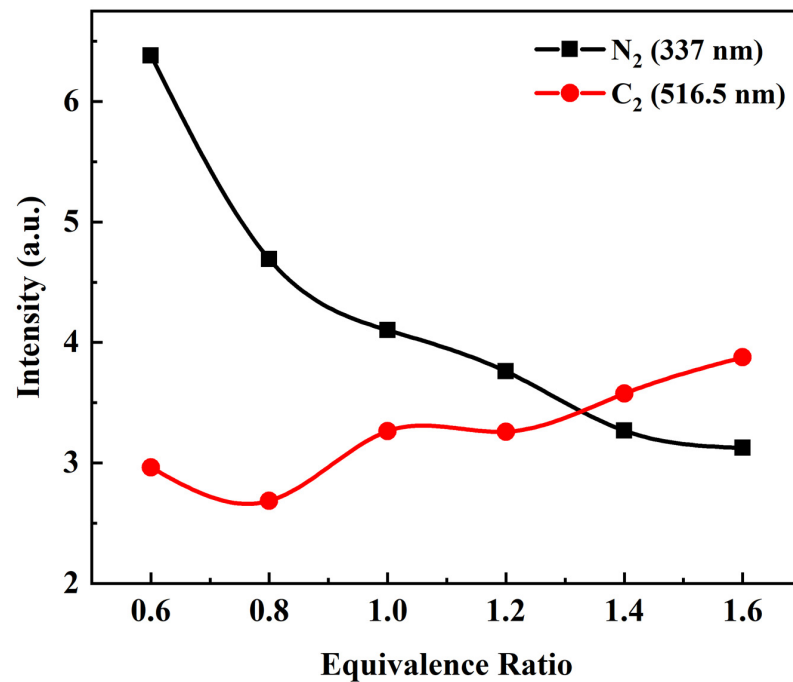


Figure 4. Variation curves of N_2 (337 nm) and C_2 (516.5 nm) signal intensities with equivalence ratio.

Figure 5 shows the calibration curve of the intensity ratio (N_2 at 337 nm to C_2 at 516.5 nm) with the equivalence ratio. In Figure 5, the X-axis represents the equivalence ratio, the Y-axis represents the intensity ratio, the scattered points are the experimental data, and the solid line is the fitting curve. In Refs [23,25,32–35], we found that the equivalence ratio measurement methods based on the intensity ratio strategy use linear fitting during the calibration process, and the scattered points in Figure 5 are approximately linear distribution, so linear fitting was also adopted by us. As can be seen, the signal intensity ratio is linearly correlated with the equivalence ratio, and the R^2 is 0.933. This indicates that the equivalence ratio measurement can be achieved based on the intensity ratio of the fluorescence signal, but the measurement uncertainty is high. We believe that the local disturbance of air will affect the signal intensity ratio and increase the uncertainty.

3.3. Equivalence Ratio Measurements Based on the Spatial Distribution of the Emission Intensity of the fs Laser-Induced Filament

In the experiments, we found that the spatial distribution of the emission signal was affected by the change of the equivalence ratio. In order to obtain the spatial distribution, the spatially resolved emission signal was determined by the following method. Before the laser experiments, it was determined that the spatial position of the spectrometer window was unchanged at different working conditions. A target with a 2×2 mm grid size was placed at the position of the filament. The target was imaged by the ICCD camera. Through calibration, it can be calculated that a pixel point represents a distance of $9 \mu\text{m}$. According

to the position of the fluorescence signal in the picture, the relative spatial position of the fluorescence signal can be calculated.

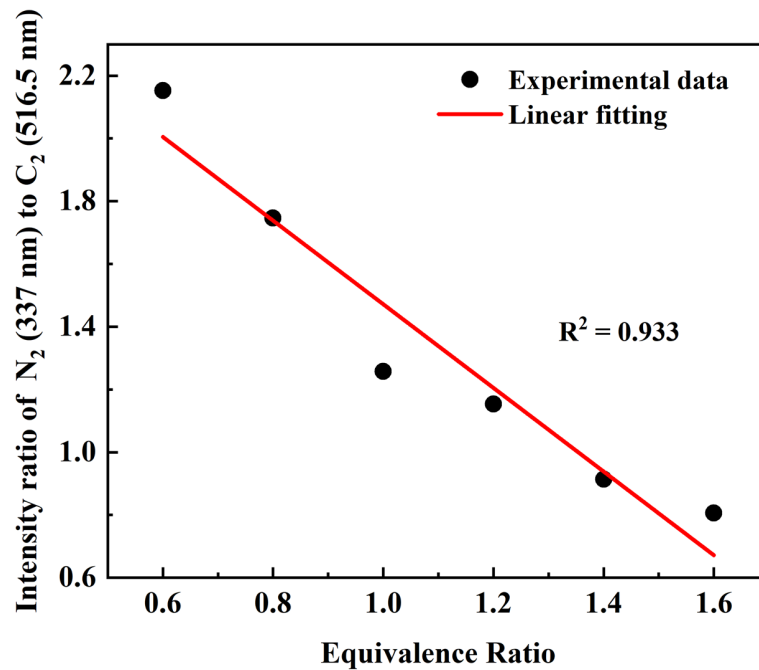


Figure 5. Calibration curve of signal intensity ratio of N₂ (337 nm) and C₂ (516.5 nm) as a function of equivalence ratio.

Figure 6 shows the spectral images and spectral curves of N₂ (337 nm) and C₂ (516.5 nm) at different equivalence ratios. The black arrow above Figure 6 represents the propagation direction of the laser (from left to right). Figure 6a,b are the spatially resolved spectra of N₂ (337 nm) and C₂ (516.5 nm) taken by the ICCD camera at different equivalence ratios, respectively. Figure 6c,d are the intensity distribution curves obtained by integrating the fluorescence signals of N₂ (337 nm) and C₂ (516.5 nm), respectively. The maximum spectral intensity at different equivalence ratios is normalized to 1 in order to more clearly display the position of peak spectral intensity at different equivalence ratios. The X-axis represents the spatial distance, and the Y-axis represents the normalized signal intensity.

It can be found in Figure 6 that, with the increase of the equivalence ratio, the peak position of both the N₂ (337 nm) signal and the C₂ (516.5 nm) signal moves towards the spherical lens (i.e., it moves from the right side to the left side). We believe that the reasons are as follows [36,37]. The peak position of the signal of the filament is determined by Equation (4).

$$f' = \frac{f \cdot Z_f}{f + Z_f} \quad (4)$$

where f' represents the peak position of the signal, f represents the focal length of the spherical lens, and Z_f represents the length of the fs laser filament. Z_f is determined by Equation (5).

$$Z_f = \frac{0.367ka^2}{\left\{ \left[(P/P_C)^{1/2} - 0.852 \right]^2 - 0.0219 \right\}^{1/2}} \quad (5)$$

where ka^2 represents the diffraction length, which is a constant related to the laser. P represents the actual power of the fs laser. The laser energy in the experiment is 2 mJ/pulse, the pulse duration is 45 fs, and the actual power is 44 GW. P_C represents the threshold power

of fs laser filamentation, expressed as the second-order nonlinear refractive index. P_C is determined by Equation (6):

$$P_C = \frac{3.72\lambda^2}{87\pi n_0 n_2}, \quad (6)$$

where λ represents the wavelength of fs laser, n_0 and n_2 represent the linear and second-order nonlinear refractive indices of the gas mixture, respectively [38,39]. The linear and second-order nonlinear refractive indices of gas mixtures are determined by the ratio of CH_4 to air ($n_{0\text{CH}_4} = 1$, $n_{0\text{air}} = 1$, $n_{2\text{CH}_4} = 1310^{-20} \text{ cm}^2/\text{W}$, $n_{2\text{air}} = 1210^{-20} \text{ cm}^2/\text{W}$).

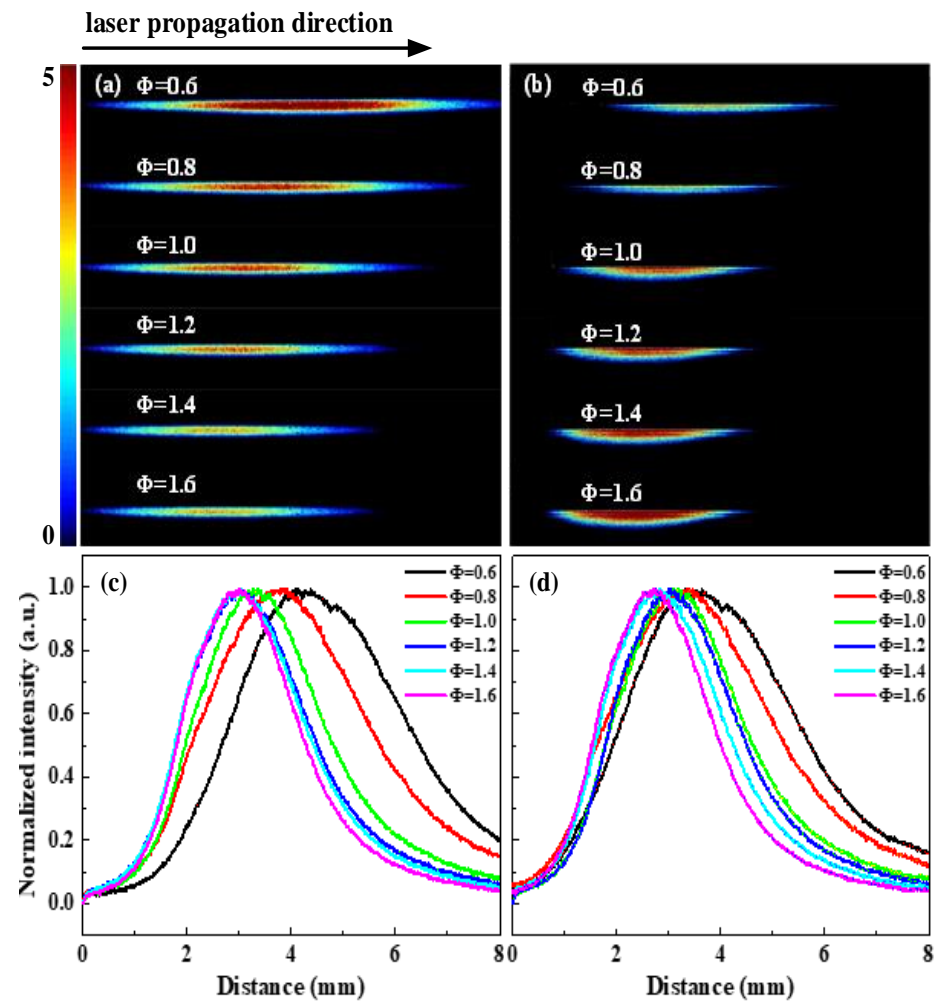


Figure 6. (a), Spectral image of N_2 (337 nm) with different equivalence ratios. (b), Spectral images of C_2 (516.5 nm) with different equivalence ratios. (c), Spatial distribution curves of N_2 (337 nm) with different equivalence ratios. (d), distribution curves of C_2 (516.5 nm) with different equivalence ratios.

According to Equations (4)–(6), with the increase of the equivalence ratio, the average second-order nonlinear refractive index increases, and the distance between the peak position of the signal and the focusing lens decreases (i.e., the peak position of the signal moves towards the spherical lens). Through calibration experiments, the equivalence ratio of the flow field can then be calculated according to the relationship between the peak position of the fluorescence signal and the equivalence ratio.

Figure 7 shows the curves of signal positions of N_2 (337 nm) and C_2 (516.5 nm) as a function of the equivalence ratio, where the signal positions are represented by the peak positions of the signals. As can be seen from Figure 7, when the equivalence ratio changes from 0.6 to 1.6, the signal positions of N_2 (337 nm) and C_2 (516.5 nm) shift by about 1.5 mm, while the mass concentration of CH_4 in the mixture increases from 3.36% to 8.48%, with a

change of only 5.12%. This indicates that the signal positions are sensitive to the change of the equivalence ratio. It can also be found from Figure 7 that the signal positions of N_2 (337 nm) and C_2 (516.5 nm) are different at the same equivalence ratio. Wu et al. [40] also found that the spatial distributions of N_2 (337 nm) and N_2^+ (428 nm) signals generated by the filament were different, which was attributed to the different generation mechanisms of N_2 (337 nm) and N_2^+ (428 nm) in the excited state. This can also explain the different signal positions of N_2 (337 nm) and C_2 (516.5 nm) at the same equivalence ratio. Compared with Figure 4, we found that the signal positions of N_2 (337 nm) and C_2 (516.5 nm) in Figure 7 change monotonically with the equivalence ratio. This is because that the peak position of the fluorescence signal is obtained by Gaussian fitting, which is not affected by local air disturbance.

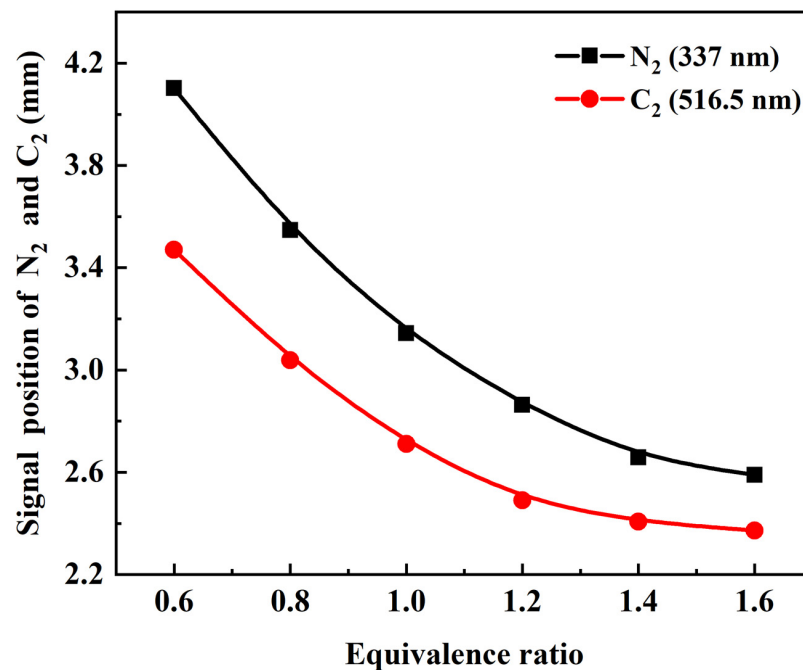


Figure 7. Variation curves of N_2 (337 nm) and C_2 (516.5 nm) signal positions with equivalence ratio.

Since the distributions of fluorescence signals are sensitive to the change of the equivalence ratio, and the spatial distributions of different fluorescence signals are different, so the equivalence ratio of the flow field can be calibrated according to the relative positions of the two different signals. The reasons for choosing the relative positions of the two different signals to calibrate the equivalence ratio are as follows: First, it can avoid the error caused by the selection of calibration origin. Secondly, it can reduce the system error caused by the optical system, such as aberration of the imaging system and photoelectric oscillation of the ICCD camera.

Figure 8 is the calibration curve of the distance between N_2 (337 nm) and C_2 (516.5 nm) signals as a function of the equivalence ratio, in which the distance between the two signals is represented by the distance between the two signal peaks. The X-axis represents the equivalence ratio, and the Y-axis represents the distance between the N_2 (337 nm) signal and the C_2 (516.5 nm) signal. The scatter points are the experimental data, and the solid line is the fitting curve. It can be seen from Figure 8 that the distance between N_2 (337 nm) and C_2 (516.5 nm) is approximately linear with the equivalence ratio, so linear fitting is conducted for the experimental data with the R^2 of 0.984. In Figure 8, the distance of N_2 (337 nm) and C_2 (516.5 nm) signals varies within a range of 0.2–0.7 mm. The ICCD camera used in the experiment has a spatial resolution of 10 μm , which can sensitively capture the distance variation caused by the change of equivalence ratio.

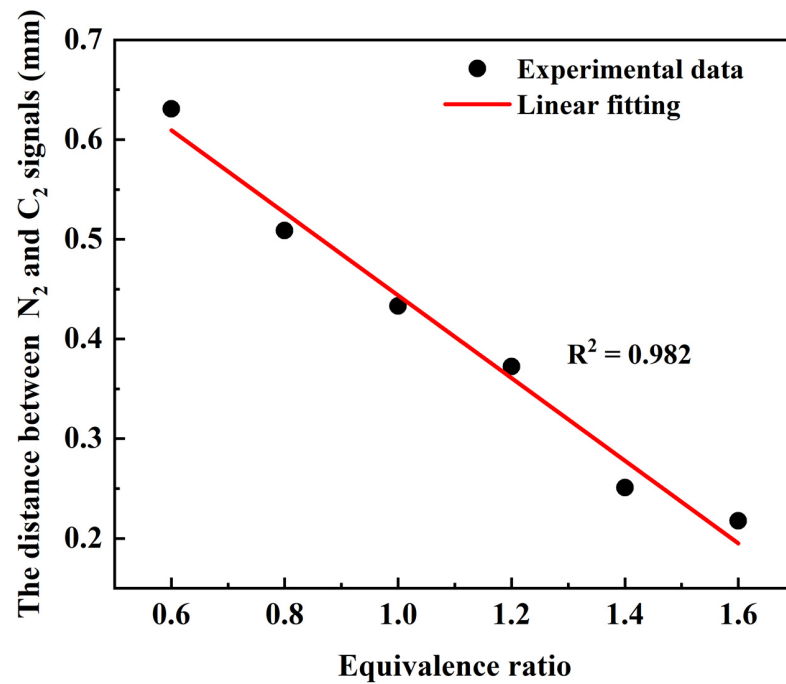


Figure 8. Calibration curve of the distance between N₂ (337 nm) and C₂ (516.5 nm) signals as a function of equivalence ratio.

To verify the accuracy of the equivalence ratio measurement, we measured the actual equivalence ratio using the calibration curve. Detailed measurement results are shown in Figure 9. The X-axis represents the actual equivalence ratio, the Y-axis represents the equivalence ratio measured in the experiments, and the scattered points in the figure are the measured results. It can be seen from Figure 9 that the measured values of the equivalence ratio match well to the actual values, indicating that the measurements based on this concept are excellent.

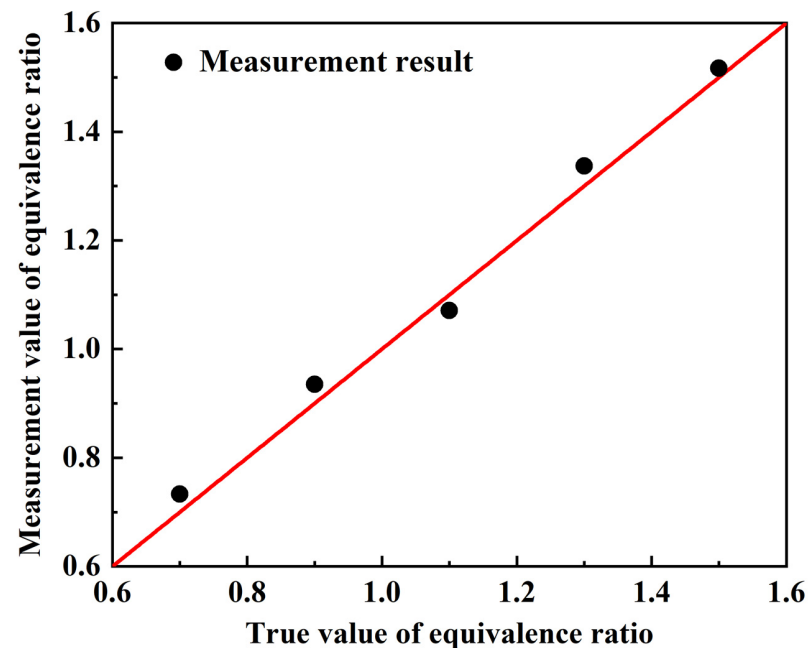


Figure 9. Verification experimental results of equivalence ratio measurement method based on signal relative position.

Compared with Figure 6, we found that both the method based on the relative position of the signals and the method based on the signal intensity ratio can be used to measure the equivalence ratio, but the method based on the relative position of the signals overcomes the interference of local air disturbance and has higher R^2 and lower measurement uncertainty. At the same time, this method provides a new idea for the measurement of the equivalence ratio of flow fields. Of course, this equivalence ratio measurement method also has some limitations. For example, this method is based on the distribution of filament to reflect the equivalence ratio of flow fields, so it can only be applied to the condition of uniform equivalent ratio.

4. Conclusions

A method for measuring the equivalence ratio based on fs laser filament is presented in this paper. A fs laser with a fundamental frequency of 800 nm was used to focus on the premixed laminar CH_4/air gas flow generated by a McKenna burner to form a filament. The spatially resolved spectra of the filament were recorded by a spectrometer, and the signals of the filament were mainly N_2 , CH, CN, C_2 , H, etc. It was found that the spatial distributions of different fluorescence signals were different and varied with the equivalence ratio. The calibration curve of the equivalence ratio was established according to the relationship between the equivalence ratio and the spatial position of N_2 (337 nm) and C_2 (516.5 nm) fluorescence signals, which was used for the equivalence ratio measurement. In this paper, the equivalence ratio measurement method based on the fluorescence signal intensity ratio is compared with the method based on the spatial distribution of the emission of the filament. This equivalence ratio measurement method has lower measurement uncertainty and provides a new idea for the equivalence ratio measurement.

Author Contributions: Conceptualization, Q.G.; methodology, B.L.; validation, M.L., J.G. and D.Z.; investigation, D.Z.; data curation, J.G.; writing—original draft preparation, M.L.; supervision, Q.G. All authors have read and agreed to the published version of the manuscript.

Funding: This research was funded by National Natural Science Foundation of China (No. 52176169 and 51806149).

Institutional Review Board Statement: Not applicable.

Informed Consent Statement: Not applicable.

Data Availability Statement: Not applicable.

Conflicts of Interest: The authors declare no conflict of interest.

References

1. Li, B.; Zhang, D.Y.; Liu, J.X.; Tian, Y.F.; Gao, Q.; Li, Z.S. A Review of Femtosecond Laser-Induced Emission Techniques for Combustion and Flow Field Diagnostics. *Appl. Sci.* **2019**, *9*, 1906. [[CrossRef](#)]
2. Aldén, M.; Bood, J.; Li, Z.S.; Richter, M. Visualization and understanding of combustion processes using spatially and temporally resolved laser diagnostic techniques. *Proc. Combust. Inst.* **2011**, *33*, 69–97. [[CrossRef](#)]
3. Allison, P.M.; Frederickson, K.; Kirik, J.W.; Rockwell, R.D.; Goynes, C.P.; Lempert, W.R.; Sutton, J.A. Flame Structure and Dynamics in a Premixed Dual-Mode Scramjet Combustor from Fluorescence Imaging. *J. Propuls. Power* **2019**, *35*, 552–564. [[CrossRef](#)]
4. Zhao, W.D.; Wang, W.G.; Li, H.Y. Numerical simulation and experimental investigation of the production of multiply charged ions by the ionization of benzene cluster with a moderate intensity laser. *Acta Phys. Sin.* **2014**, *63*, 103602.
5. Richardson, D.R.; Jiang, N.; Blunck, D.L.; Gord, J.R.; Roy, S. Characterization of inverse diffusion flames in vitiated cross flows via two-photon planar laser-induced fluorescence of CO and 2-D thermometry. *Combust. Flame* **2016**, *168*, 270–285. [[CrossRef](#)]
6. Chan, V.S.S.; Turner, J.T. Velocity measurement inside a motored internal combustion engine using three-component laser Doppler anemometry. *Opt. Laser Technol.* **2000**, *32*, 557–566. [[CrossRef](#)]
7. Braun, A.; Korn, G.; Liu, X.; Du, D.; Mourou, G. Self-channeling of high-peak-power femtosecond laser pulses in air. *Opt. Lett.* **1995**, *20*, 73–75. [[CrossRef](#)]
8. Spence, D.E.; Kean, P.N.; Sibbett, W. 60-fsec pulse generation from a self-mode-locked Ti:sapphire laser. *Opt. Lett.* **1991**, *16*, 42–44. [[CrossRef](#)]
9. Chen, X.W.; Liu, J.; Zhu, Y.; Leng, Y.X.; Ge, X.C.; Li, R.X.; Xu, Z.Z. Self-compression of femtosecond pulses in argon with a power close to the self-focusing threshold. *Chin. Phys. B* **2008**, *17*, 1826–1832.

10. Li, H.L.; Chu, W.; Xu, H.L.; Cheng, Y.; Chin, S.L.; Yamanouchi, K.; Sun, H.B. Simultaneous identification of multi-combustion-intermediates of alkanol-air flames by femtosecond filament excitation for combustion sensing. *Sci. Rep.* **2016**, *6*, 27340. [[CrossRef](#)]
11. Li, H.L.; Xu, H.L.; Yang, B.S.; Chen, Q.D.; Zhang, T.; Sun, H.B. Sensing combustion intermediates by femtosecond filament excitation. *Opt. Lett.* **2013**, *38*, 1250–1252. [[CrossRef](#)]
12. Brodeur, A.; Chin, S.L. Ultrafast white-light continuum generation and self-focusing in transparent condensed media. *J. Opt. Soc. Am. B* **1999**, *16*, 637–650. [[CrossRef](#)]
13. Kosareva, O.G.; Kandidov, V.P.; Brodeur, A.; Chien, C.Y.; Chin, S.L. Conical emission from laser–plasma interactions in the filamentation of powerful ultrashort laser pulses in air. *Opt. Lett.* **1997**, *22*, 1332–1334. [[CrossRef](#)]
14. Luo, Q.; Liu, W.; Chin, S.L. Lasing action in air induced by ultra-fast laser filamentation. *Appl. Phys. B Lasers Opt.* **2003**, *76*, 337–340. [[CrossRef](#)]
15. Couairon, A.; Mysyrowicz, A. Femtosecond filamentation in transparent media. *Phys. Rep.* **2007**, *441*, 47–189. [[CrossRef](#)]
16. Li, H.L.; Xu, H.L. Ultrafast strong laser filamentation and applications in high-temperature combustion field. *Chin. Sci. Bull.* **2017**, *62*, 2876–2885. [[CrossRef](#)]
17. Li, H.L.; Wei, X.Y.; Xu, H.L.; Chin, S.L.; Yamanouchi, K.; Sun, H.B. Femtosecond laser filamentation for sensing combustion intermediates: A comparative study. *Sens. Actuators B Chem.* **2014**, *203*, 887–890. [[CrossRef](#)]
18. Li, B.; Tian, Y.F.; Gao, Q.; Zhang, D.Y.; Li, X.F.; Zhu, Z.F.; Li, Z.S. Filamentary anemometry using femtosecond laser-extended electric discharge—FALED. *Opt. Express.* **2018**, *26*, 21132–21140. [[CrossRef](#)]
19. Li, S.Y.; Zhang, D.Y.; Gao, Q.; Li, B.; He, Y.; Wang, Z.H. Temperature measurement in combustion flow field with femtosecond laser-induced filament. *Acta Phys. Sin.* **2020**, *69*, 234207.
20. Li, Y.; Gao, W.; Zhang, P.; Fu, Z.; Cao, X. Influence of the equivalence ratio on the knock and performance of a hydrogen direct injection internal combustion engine under different compression ratios. *Int. J. Hydrog. Energy* **2021**, *46*, 11982–11993. [[CrossRef](#)]
21. Wang, X.; Jin, T.; Luo, K.H. Response of heat release to equivalence ratio variations in high karlovitz premixed H₂/air flames at 20 atm. *Int. J. Hydrog. Energy* **2019**, *44*, 3195–3207. [[CrossRef](#)]
22. Al-Farayedhi, A.A.; Antar, M.A.; Khan, A. Effect of the equivalence ratio on the concentration of CH₄/NO₂/O₂ combustion products. *Int. J. Energy Res.* **2015**, *23*, 1165–1175. [[CrossRef](#)]
23. Zhang, D.Y.; Gao, Q.; Li, B.; Zhu, Z.F.; Li, Z.S. Instantaneous one-dimensional equivalence ratio measurements in methane/air mixtures using femtosecond laser-induced plasma spectroscopy. *Opt. Express.* **2019**, *27*, 2160. [[CrossRef](#)]
24. Kasparian, J.; Wolf, J.P. Physics and applications of atmospheric nonlinear optics and filamentation. *Opt. Express.* **2008**, *16*, 466–493. [[CrossRef](#)]
25. Zang, H.W.; Yao, D.W.; Wang, S.Q.; Fu, Y.; Zhang, W.; Chen, S.M.; Li, H.L.; Xu, H.L. In situ determination of the equivalence ratio in a methane/air flow field by femtosecond filament excitation. *Laser Phys.* **2020**, *30*, 035402. [[CrossRef](#)]
26. Simek, M.; Babický, V.; Clupek, M.; Sunka, P. Observation of the N₂ Herman infrared system in pulsed positive streamer induced emission at atmospheric pressure. *J. Phys. D Appl. Phys.* **2001**, *34*, 3185–3190. [[CrossRef](#)]
27. Keith, S.; Martin, S. CH and C₂ Measurements Imply a Radical Pool within a Pool in Acetylene Flames. *J. Phys. Chem. A* **2007**, *111*, 2098–2114.
28. Xu, H.L.; Azarm, A.; Bernhardt, J.; Kamali, Y.; Chin, S.L. The mechanism of nitrogen fluorescence inside a femtosecond laser filament in air. *Chem. Phys.* **2009**, *360*, 171–175. [[CrossRef](#)]
29. Kong, F.; Luo, Q.; Xu, H.L.; Sharifi, M.; Song, D.; Chin, S.L. Explosive photodissociation of methane induced by ultrafast intense laser. *J. Chem. Phys.* **2006**, *125*, 133320. [[CrossRef](#)] [[PubMed](#)]
30. Pintassilgo, C.D.; Cernogora, G.; Loureiro, J. Spectroscopy study and modelling of an afterglow created by a low-pressure pulsed discharge in N₂–CH₄. *Plasma Sources Sci. Technol.* **2001**, *10*, 147–161. [[CrossRef](#)]
31. Li, B.; Zhang, D.Y.; Li, X.F.; Gao, Q.; Zhu, Z.F.; Li, Z.S. Femtosecond laser-induced cyano chemiluminescence in methane-seeded nitrogen gas flows for near-wall velocimetry. *J. Phys. D Appl. Phys.* **2018**, *51*, 295102. [[CrossRef](#)]
32. Zimmer, L.; Tachibana, S. Laser induced plasma spectroscopy for local equivalence ratio measurements in an oscillating combustion environment. *Proc. Combust. Inst.* **2007**, *31*, 737–745. [[CrossRef](#)]
33. Joshi, S.; Olsen, D.B.; Dumitrescu, C.; Puzinauskas, P.V.; Yalin, A.P. Laser-induced breakdown spectroscopy for in-cylinder equivalence ratio measurements in laser-ignited natural gas engines. *Appl. Spectrosc.* **2009**, *63*, 549–554. [[CrossRef](#)]
34. Zhang, S.H.; Yu, X.L.; Li, F.; Kang, G.J.; Chen, L.H.; Zhang, X.Y. Laser induced breakdown spectroscopy for local equivalence ratio measurement of kerosene/air mixture at elevated pressure. *Opt. Lasers Eng.* **2012**, *50*, 877–882. [[CrossRef](#)]
35. Kammermann, T.; Merotto, L.; Bleiner, D.; Soltic, P. Spark-induced breakdown spectroscopy for fuel-air equivalence ratio measurements at internal combustion engine-relevant conditions. *Spectrochim. Acta Part B At. Spectrosc.* **2019**, *155*, 79–89. [[CrossRef](#)]
36. Liu, W.; Chin, S.L. Direct measurement of the critical power of femtosecond Ti:sapphire laser pulse in air. *Opt. Express* **2005**, *13*, 5750–5755. [[CrossRef](#)] [[PubMed](#)]
37. Li, H.L.; Chu, W.; Zang, H.W.; Xu, H.L.; Cheng, Y.; Chin, S.L. Critical power and clamping intensity inside a filament in a flame. *Opt. Express* **2016**, *24*, 3424–3431. [[CrossRef](#)] [[PubMed](#)]
38. Lorient, V.; Hertz, E.; Faucher, O.; Lavorel, B. Measurement of high order Kerr refractive index of major air components: Erratum. *Opt. Express* **2010**, *18*, 3011–3012. [[CrossRef](#)]

-
39. Shaw, M.J.; Hooker, C.J.; Wilson, D.C. Measurement of the nonlinear refractive index of air and other gases at 248 nm. *Opt. Commun.* **1993**, *103*, 153–160. [[CrossRef](#)]
 40. Wu, J.B.; Wu, Z.Y.; Chen, T.; Zhang, H.; Zhang, Y.F.; Zhang, Y.; Lin, S.; Cai, X.M.; Chen, A.M.; Jiang, Y.F.; et al. Spatial distribution of the fluorescence induced by femtosecond laser filamentation in ambient air. *Opt. Laser Technol.* **2020**, *131*, 106417. [[CrossRef](#)]